Smart Structures and Materials, 2004, Vol. 13, No. 4, pp888-895

Title of Article

Characterisation of the response of fibre Bragg gratings fabricated in stress and geometrically induced high birefringence fibres to temperature and transverse load.

Authors and addresses

Edmon Chehura, Chen-Chun Ye, Stephen E. Staines, Stephen W. James, and Ralph P. Tatam*

Optical Sensors Group, Centre for Photonics and Optical Engineering, School of Engineering, Cranfield University, Cranfield, Bedford, MK43 0AL, UK.

Tel: +44 1234 754630

Fax: +44 1234 751566

Email: r.p.tatam@cranfield.ac.uk

*Correspondence author

Short Title

HiBi fibre Bragg grating response to temperature and transverse load.

PACS classification

42.81.-i

42.81.Pa

42.81.Gs

Abstract

The transverse load and temperature sensitivities of fibre Bragg gratings (FBG) fabricated in a range of commercially available stress and geometrically induced high birefringent (HiBi) fibres have been experimentally investigated. The wavelength reflected by the FBG in each polarisation eigenmode was measured independently and simultaneously using a custom designed interrogation system. The highest transverse load sensitivity, of 0.23 ±0.02 nm/(N/mm), was obtained with HiBi FBGs fabricated in elliptically clad fibre. This was ~25% higher than for any other HiBi fibre, which, coupled with the small diameter of the fibre, makes it a good candidate for an embedded or surface mounted strain sensor. The highest temperature sensitivity of 16.5 ± 0.1 pm/^{0}C, approximately 27% greater than any other fibre type, was obtained with the HiBi FBG fabricated in Panda fibre. HiBi FBG sensors fabricated in D-clad fibre were the only ones to exhibit identical temperature sensitivities for the slow and fast axes (11.5 ± 0.1 pm/^{0}C).

Key Words

Transverse strain, birefringent fibres, multi-axial strain, 3D strain, temperature, fibre Bragg grating sensors

1. Introduction

A fibre Bragg grating (FBG) is a periodic modulation of the refractive index within the core of an optical fibre and acts to couple a forward propagating fibre core mode to a backward propagating core mode at a particular wavelength given by

$$\lambda_B = 2n_{eff}\Lambda \qquad (1)$$

where λ_B, n_{eff}, and Λ are the reflected Bragg wavelength, effective refractive index, and the grating period respectively. A change in the effective refractive index and/or the grating period will cause a shift in the reflected Bragg wavelength. This has led to FBGs being investigated in a wide range of applications for the measurement of strain and to a lesser extent temperature [1-3]. However, the majority of applications have related the change in Bragg wavelength, generally measured using an optical spectrometer, to axial strain and/or temperature acting on the FBG [4-6]. More recently there has been an interest in measuring the transverse strain components in addition to the axial strain with the goal of internal stress measurements in composite materials. Applications for this more complex approach include structural health monitoring [7], impact and damage detection [8], and cure monitoring of composite materials [9,10]. FBG sensors fabricated in high linearly birefringent (HiBi) fibres are ideal for these measurements and have been proposed for the measurement of multi-strain components [11].

The reflection spectrum from a FBG fabricated in HiBi fibre will consist of two Bragg peaks, one in each of the two polarisation axes of the fibre. It has been proposed that the three components of strain and temperature could be measured by co-locating another FBG with a sufficiently different centre wavelength [12]. The result is a system of four simultaneous equations that can be solved for the 4 unknowns using experimental calibration data [13]. The working principle of a HiBi FBG sensor was demonstrated recently in curing composites [10,14]. There has been a limited number of

investigations of the response of HiBi FBG sensors to applied transverse load [12,15-19] and these have focused mainly on elliptical cladding (3M [20]) and bow tie (Fibercore [21]) fibres. There has not been any temperature characterisation of HiBi FBG sensors reported.

This paper presents the characterisation of FBG sensors, fabricated in both stress and geometrically induced HiBi fibres, to applied transverse load and temperature.

2. Birefringence in optical fibres

Most fibre optic applications, such as telecommunications and sensors, demand coherent optical transmission, which requires systems capable of controlling the polarisation state of the light [22,23]. Fibres that are capable of maintaining the polarisation of the coupled light can be classified either as high birefringent or low birefringent fibres. Linearly polarised or circularly polarised waves propagate with small polarisation dispersion in low birefringence fibre but the polarisation state is sensitive to external perturbations such as bends, twists, and temperature, which induce additional birefringence whose magnitude is comparable to or greater than the intrinsic birefringence. When the intrinsic birefringence is deliberately enhanced to be very large in comparison to that from external perturbations, the result is a fibre with high birefringence that maintains the state of polarisation of light that is matched to a polarisation eigen mode (linear or circular depending on the nature of the induced birefringence) of the fibre.

For non-HiBi fibres subjected to a transverse load the birefringence, B_f, is given by [24]

$$B_f = 2k_o n_o^{\,3}\left(p_{11} - p_{12}\right)\left(1 + \nu_p\right)\cdot\frac{F}{\pi r E} \qquad (2)$$

where k_o, n_o, v_p, r, E, F, p_{11} and p_{12} are respectively the free space propagation constant, average refractive index of the fibre, Poisson ratio, outer radius of the fibre, Young's modulus, force per unit length, and the elasto-optic coefficients of the fibre. Equation (2) indicates that the application of a transverse load will alter the birefringence of the fibre.

Internal birefringence of the fibre is produced by various mechanisms either based on the geometric effect of the core or on a stress effect around the core [24,25]. Birefringence is induced in the core whenever its circular symmetry is broken, thus producing an anisotropic refractive index distribution. Such fibres usually have an elliptically shaped core [26] although other types, e.g. dumbell core, have been fabricated [27]. Stress induced birefringent fibres are produced from asymmetric transverse stress which introduces linear birefringence through elasto-optic refractive index changes in the core [25]. The stress is frozen internally in the fibre during fabrication as the result of different thermal contraction between differently doped regions of the fibre located symmetrically on either side of the core. Elliptical cladding fibres, elliptical jacket fibres, PANDA fibres, and bow-tie fibres are examples of stress induced birefringent fibres. Figure 1 shows schematics of the HiBi fibres that were used in this work. The slow axis is the axis or plane in which the stress applying parts or the major axis of the ellipse lie.

The modal birefringence B is the difference in the effective refractive indices between the two orthogonal modes of the fibre. Birefringence is usually characterised by its beat length L_p, which is the distance after which the input polarisation state is reproduced as the polarisation state evolves along the length of the fibre, that is, the relative phase of the light propagating in the two orthogonal polarisation modes change by 2π.

$$L_p = \frac{\lambda}{B} = \frac{2\pi}{\Delta\beta} \qquad (3)$$

where λ and $\Delta\beta$ are the optical wavelength and the change in the mode propagation constant respectively. The shorter the beat length, the higher the birefringence. Modal birefringence, produced by all kinds of internal origins in the high birefringent fibres, is given by [25]

$$B = B_G + B_{SO} + B_S \qquad (4)$$

where B_G is the geometric component of the birefringence introduced by the shape of the core, B_{SO} is the self-stress component, and B_S is the outer stress component. The self-stress component of the birefringence is induced by the thermal expansion difference of the asymmetrical core of the fibre. The outer stress component is introduced from outside the core e.g. by elliptical cladding/jacket or stress applying parts. The birefringence components have been calculated [25] but a knowledge of the physical properties and geometry of the fibres is required which are, in general, unavailable from commercial manufacturers.

3. Experiment

FBG sensors were fabricated in our laboratories into hydrogen loaded stress and geometrically induced HiBi fibres using an injection-seeded frequency-quadrupled Nd:YAG laser operating at a wavelength of 266 nm. A two-beam, three mirror interferometric technique [28] was used to fabricate FBG sensors of length 5 mm. The HiBi fibre was aligned such that the laser illumination avoided the stress lobes for the case of stress-induced HiBi fibres. The axes of the stress induced HiBi fibre were identified through observation of the diffraction pattern from the fibre when illuminated from the side with a Helium Neon laser source [29]. This method could not, however, be used for geometrically induced HiBi fibres as the diffraction pattern from the two polarisation

axes was not sufficiently distinctive. The eigen axes of these fibres, apart from the D-clad fibre whose axes are known from the shape of the fibre (Figure 1), had to be identified visually by looking at a polished fibre end through a microscope. The FBG sensors were subjected to transverse stress using a loading fixture designed to minimise fibre rotation (Figure 2).

The load applied to the FBG sensor was detected using a FUTEK miniature load button with a capacity of 222 N and resolution of 0.1 N. The output of the load button was recorded through the data acquisition (DAQ) card simultaneously with the wavelength shifts of the gratings using an interrogation system [16] based on a scanning fibre Fabry-Perot (FFP) interferometer coupled to high birefringent fibre (Figure 3). The super luminescent diode had a 3 dB bandwidth of 50 nm centred at 1560 nm and the measured output power at the fibre pigtail was 0.6 mW. The FFP filter had a finesse of 895 and free spectral range of 5330 GHz (~42.7 nm). The overall extinction ratio of the interrogation system was measured to be 15 ± 0.5 dB. The wavelength resolution of the system was determined from the standard deviation to be 2 pm. A key attribute of this instrument is that it measures independently and simultaneously the wavelength reflected by the Bragg grating in each polarisation eigenmode.

A pair of rotational stages, with angular resolution of 2^0, was used to rotate the HiBi fibre containing the FBG sensors to determine the sensitivity as a function of the orientation of the eigen axes with respect to the applied load. The length of the stripped fibre section subjected to transverse load was 24 mm and both the test and support fibres were of the same fibre type. The test and support fibres for the D-clad fibre were aligned identically and both fibres were rotated. This minimised the variation in the fibre height above the bottom plate thereby minimising fibre rotation. The reference angle (0^0) for the rotation was not made coincident with either of the eigen axes of the fibre but was arbitrarily chosen.

The responses of the HiBi FBG sensors to temperature were investigated by placing the sensors in a tube temperature furnace such that there was no strain applied to the sensors. The temperature furnace was fitted with a Eurotherm PID temperature controller. The temperature of the furnace was incremented in steps of 10 ^{0}C from room temperature to about 150 ^{0}C and the data, which was averaged over 30 seconds, was recorded after the system reached a steady state. The temperature stability of the furnace in the steady state was 0.2 ^{0}C. Measurements were also taken as the system was cooled down to room temperature.

4. Results and Discussion

FBGs were fabricated in the six HiBi fibre types shown schematically in Figure 1 and listed in Table 1. The fibre parameters are shown in Table 2 and the measured wavelength separation of the slow and fast axis FBG peaks are summarised in Table 3.

The comparison of the responses of the FBG sensors in elliptical core and elliptical clad HiBi fibres is shown in Figure 4. The maximum and minimum load sensitivities in the slow and fast axis are significantly higher in the elliptical clad fibre. Figure 5 is a similar comparison of Panda and TruePhase fibres, both of which use stress rods to generate the birefringence. The maximum load sensitivities for the slow axis of each fibre are similar while the minimum sensitivities in the fast axes are different. In Figure 6 the maximum sensitivities for the FBG sensors in Bow tie and D-clad fibres are shown to be the same, within experimental error, but the minimum sensitivity of the D-clad fibre is significantly higher.

The load sensitivity is plotted as a function of the angle of rotation of the HiBi fibre containing the FBG sensors in Figures 7-9. The maximum and minimum sensitivities are obtained when the load was applied along an eigen axis. This method has also been used to confirm the orientation of the eigen axes of the HiBi fibres, determined as discussed in section 3.

Table 4 gives a summary of the load sensitivities of the FBG sensors fabricated in different types of HiBi fibre when subjected to transverse load. The maximum sensitivity was obtained when the load was applied along an eigen axis of the fibre. The elliptical clad fibre exhibited the highest sensitivity, and this was found in the slow axis. The elliptical clad fibre also showed maximum sensitivity in the fast axis when compared to the other fibre types. In general, the maximum sensitivity of the slow axis is higher than that of the fast axis with the exception of the Panda and elliptical core fibres whose slow and fast axis maximum load sensitivities have similar magnitudes. The greatest differential transverse load sensitivity was measured between the eigen axes of the bow tie fibre.

The high sensitivity of the elliptical clad fibre may be attributed to its smaller diameter (80 μm) as well as to the presence of additional stress around the core created by the elliptical cladding during the manufacturing process. The stresses along the major diameter of the cladding are greater than those along the minor axis direction and this is probably the reason the sensitivity in the slow axis of this fibre is greater when compared to that of the fast axis. The fact that the elliptical cladding creates some stress along the minor axis may be the reason the elliptical clad fibre has higher transverse strain sensitivity in its fast axis when compared to other fibre types.

There is no additional stress transferred to the core of the elliptical core fibre from its cladding and this is probably the reason the transverse strain sensitivities for this fibre are similar for both the

slow and fast axes. It is not easy to infer why the Panda fibre has similar transverse strain sensitivities for its fast and slow axes. One possibility is that the stress generated by the stress rods of this fibre may be less concentrated along the slow axis when compared to other fibres that use stress applying parts (SAPs) since its stress rods are further away from the core (Figure 1).

Figures 10 - 15 are plots of FBG wavelength shifts as a function of the temperature applied to FBGs fabricated in the different types of HiBi fibre. The graphs show plots of the response to temperature of the FBGs in both the slow and fast axes of the HiBi fibres. The continuous lines represent the measured temperature in the fast axis while the dashed lines are for the slow axis. Lines have been omitted in Figure 10 for clarity, since the two graphs are nearly matched.

Table 5 shows the various HiBi FBG sensors' sensitivities to applied temperature. The responses are linear with R^2 values of at least 0.999. The results show that the slow and fast axes of the fibres do not have the same temperature sensitivities. The fast axes of the HiBi fibre are generally more sensitive to temperature than the slow axes. The FBG sensors in the stress induced HiBi fibres have higher sensitivities to temperature than those fabricated in the geometrically induced HiBi fibres. The FBGs fabricated in Panda fibre were the most sensitive to temperature. Furthermore the FBG sensors in the D-clad HiBi fibre have approximately identical temperature sensitivities for the slow and fast axes of the fibre. The greatest differential temperature sensitivity was measured between the eigen axes of the elliptical clad fibre.

The thermal expansion coefficients of the core and cladding are nearly the same, hence the fast axis of fibres with no SAPs or of fibres with the smallest dimension becomes more sensitive to temperature when compared to the slow axis, where the SAPs have a higher thermal expansion coefficient. The thermal stress that was frozen internally in the fibre (due to SAPs) during

fabrication may be released by an increase in temperature thus adding to the temperature sensitivity of the stress induced HiBi fibres and making them more sensitive than the geometrically induced HiBi fibres. The matched temperature sensitivities of the slow and fast axes of the D-clad fibre is probably linked to the D shape of the fibre, since without the D cladding the fibre would have behaved as the normal elliptical core fibre.

The response of a HiBi FBG sensor to external stimuli is generally considered to be a function of three orthogonal strain components and temperature, a total of four unknowns. Thus a total of four FBG sensors, from two co-located HiBi FBGs, will be required to determine the four unknowns from a system of four simultaneous equations. The asymmetric shape of the D-clad fibre could be useful for fibre alignment during lay up in composite materials. If the fibre is laid with its flat face resting in the plane of the specimen, this is likely to minimise any fibre rotation that could change the orientation of the eigen axes. Such a rotation, if not accounted for, could result in the measurements being interpreted as having shear strain.

5. Conclusion

FBG sensors were fabricated in stress and geometrically induced birefringent fibres and the slow and fast axis wavelength separation range was 0.35 – 0.6 nm. The FBG sensors were subjected to known transverse loads at various orientations of the fibre in the range 0 - 180^0. The transverse load sensitivity of the FBG sensors in the slow axis of the fibre was higher than that of the fast axes. The highest sensitivity of the FBG sensor is therefore associated with the transverse plane having the longest geometry or the transverse plane in which anisotropy exists. The elliptical clad fibre exhibited the highest overall transverse load sensitivity, ~ 25% higher than any of the other fibre

types. Consequently the high sensitivity of this fibre makes it an ideal sensor for both surface and embedded multi-axial strain sensing in which a high strain transfer coefficient is required.

The FBGs were subsequently subjected to temperature loads in the range from room temperature to about 150 ^{0}C and their responses were found to be linear with R^2 values of at least 0.999. In contrast to the transverse strain results, the temperature sensitivities of the FBG sensors measured in the fast axis of the HiBi fibres was higher compared to that measured in the slow axis. The Panda fibre exhibited the highest overall temperature sensitivity, ~ 27 % higher than any of the other fibre types. An interesting result was the matched temperature sensitivities of the fast and slow axes of the HiBi FBG sensor in D-clad fibre. The results of our experiments confirm that the method currently proposed to measure 3D strain and temperature by co-locating two HiBi FBGs at two different wavelengths is applicable.

Acknowledgements

This work was supported by the Engineering and Physical Sciences Research Council, UK (GR/M89454).

References

1. Y. J. Rao, 1999, "Recent progress in applications of in-fibre Bragg grating sensors", *Opt. Laser. Eng.*, **31**, pp. 297-324.
2. S. W. James, M. L. Dockney, and R. P. Tatam, 1996, "Simultaneous independent temperature and strain measurement using in-fibre Bragg grating sensors", *Electron. Lett.*, **32**(12), pp. 1133-1134.
3. H. B. Liu, H. Y. Liu, G. D. Peng, and P. L. Chu, 2003, "Strain and temperature sensor using a combination of polymer and silica fibre Bragg gratings", *Opt. Comm.*, **219**, pp. 139-142.
4. M. G. Xu, J. –L. Archambault, L. Reekie, and J. P. Dakin, 1994, "Discrimination between strain and temperature effects using dual-wavelength fibre grating sensors", *Electron. Lett.*, **30**(13), pp. 1085-1087.
5. Y. J. Rao, S. F. Yuan, X. K. Zeng, D. K. Lian, Y. Zhu, Y. P. Wang, S. L. Huang, T. Y. Liu, G. F. Fernando, L. Zhang, and I. Bennion, 2002, "Simultaneous strain and temperature measurement of advanced 3-D braided composite materials using an improved EFPI/FBG system", *Opt. Laser. Eng.*, **38**, pp. 557-566.
6. H-K. Kang, D-H. Kang, C-S. Hong, and C-G. Kim, 2003, "Simultaneous monitoring of strain and temperature during and after cure of the unsymmetric composite laminate using fibre-optic sensors", *Smart Mater. Struct.*, **12**, pp. 29-35.
7. M. P. Whelan, D. Albrecht, and A. Capsoni, 2002, "Remote structural monitoring of the Cathedral of Como using an optical fibre Bragg grating sensor system", *Proc. SPIE*, **4694**, pp. 242-252.
8. N. Takeda, Y. Okabe, R. Tsuji, and S. Takeda, 2002, "Application of chirped fibre Bragg grating sensors for damage identification in composites", *Proc. SPIE*, **4694**, pp. 106-117.

9. J.-Y. Chen, S. V. Hoa, C.-K. Jen, and H. Wang, 1999, “Fibre-optic and ultrasonic measurements for in-situ cure monitoring of graphite/epoxy composites”, *J. Compos. Mater.*, **33**(20), pp. 1860-1881.
10. E. Chehura, A. Skordos, C-C. Ye, S. W. James, I. Partridge, and R. P. Tatam, 2003, “Multi-axial strain monitoring in curing glass fibre/epoxy composites measured using fibre Bragg grating sensors fabricated in high birefringent fibres”, *16th Int. Conf. on Optical Fiber Sensors (Nara, Japan)*, (Japan: IEICE), pp. 180-183.
11. E. Udd, W. Schulz, J. Seim, E. Haugse, A. Trego, P. Johnson, T. E. Bennett, D. Nelson, and A. Makino, 2000, “Multidimensional strain field measurements using fibre optic grating sensors”, *Proc. SPIE*, **3986**, pp. 255-262.
12. C. M. Lawrence, D. V. Nelson, E. Udd, and T. Bennett, 1999, “A fibre optic sensor for transverse strain measurement”, *Exp. Mech.*, **39**(3), pp. 202-209.
13. D. Nelson, A. Makino, C. Lawrence, J. Seim, W. Schulz, and E. Udd, 1998, “Determination of the K-Matrix for the multi-parameter fiber grating sensor in AD072 Fibercore fiber”, *Proc. SPIE*, **3489**, pp. 79-85.
14. E. Udd, K. Black, W. Schulz, S. Kreger, M. Kunzler, and D. Heider, 2002, “In-situ evaluation of composite structural performance in presence of high stress/strain gradients using multi-axis fibre grating strain sensors”, *15th Int. Conf. on Optical Fiber Sensors (Portland OR, USA)*, (USA: IEEE), pp. 59-62.
15. E. Udd, D. Nelson, and C. Lawrence, 1997, “Multiple axis strain sensing using fiber gratings written onto birefringent single mode optical fibre”, *12th Int. Conf. on Optical Fiber Sensors (Williamsburg, USA)*, (Washington, DC: OSA), pp. 48-51.
16. C- C. Ye, S. E. Staines, S. W. James, and R. P. Tatam, 2002, “A polarisation-maintaining fibre Bragg grating interrogation system for multi-axis strain sensing”, *Meas. Sci. Technol.*, **13**(9), pp. 1446-1449.

17. F. Bosia, P. Giaccari, M. Facchini, J. Botsis, H. Limberger, and R. Salathe, 2002, "Characterisation of embedded fiber Bragg grating sensors written in high-birefringent optical fibres subjected to transverse loading", *Proc. SPIE*, **4694**, pp. 175-186.
18. I. Abe, R. E. de Goes, J. L. Fabris, H. J. Kalinowski, M. Muller, M. C. Fujihara, R. Falate, B. W. Diesel, R. C. Kamikawachi, and C. L. Barbosa, 2003, "Production and characterization of refractive index gratings in high-birefringence fibre optics", *Opt. Laser. Eng.*, **39**, pp. 537-548.
19. E. Chehura, C-C. Ye, S. W. James, and R. P. Tatam, 2003, "Characterisation of the response of fibre Bragg grating sensors written in different types of high birefringent fibres subjected to transverse load.", *16th Int. Conf. on Optical Fiber Sensors (Nara, Japan)*, (Japan: IEICE), pp. 240-243.
20. 3M United Kingdom PLC, 3M Centre, Cain Road, Bracknell, RG12 8HT, United Kingdom.
21. Fibercore Limited, Fibercore House, University Parkway, Chilworth Science Park, Southampton, Hampshire, SO16 7QQ, UK.
22. T. Okoshi, 1987, "Recent advances in coherent optical fiber communication systems", *J. Lightwave Technol.*, **LT-5**(1), pp. 44-51.
23. D. N. Payne, 1984, "Fibers for sensors", *Proc. SPIE Int. Soc. Opt. Eng.*, **514**, pp. 353-360.
24. S. C. Rashleigh, 1983, "Origins and control of polarization effects in single-mode fibers", *J. Lightwave Technol.*, **LT-1**(2), pp. 312-331.
25. J. Noda, K. Okamoto, and Y. Sasaki, 1986, "Polarization-maintaining fibers and their applications", *J. Lightwave Technol.*, **LT-4**(8), pp. 1071-1089.
26. R. B. Dyott, J. R. Cozens, and D. G. Morris, 1979, "Preservation of polarization in optical-fiber waveguides with elliptical cores", *Electron. Lett.,* **15**(13), pp. 380-382.
27. V. Ramaswamy, W. G. French, and R. D. Standley, 1978, "Polarisation characteristics of noncircular core single-mode fibers", *Appl. Opt.*, **17**(18), pp. 3014-3017.

28. G. Meltz, W. W. Morey, and W. H. Glenn, 1989, “Formation of Bragg gratings in optical fibres by transverse holographic method”, *Opt. Lett.*, **14**(15), pp. 823.
29. C. N. Pannell, R. P. Tatam, J. D. C, Jones, and D. A. Jackson, 1988, “A fibre-optic frequency shifter utilising travelling flexure waves in birefringent fibre”, *The J. of the Inst. of Electronic and Radio Engineers*, supplement to vol. **58**(5), S92-S98.
30. KVH Industries, Inc., Fiber Optic Group, KVH Headquarters**,** 50 Enterprise Center, Middletown, RI 02842 USA.
31. OFS Fitel Denmark I/S, Priorparken 680, DK-2605 Brøndby, Denmark.
32. Fujikura Europe Ltd, Electronics and Fibre Optics, C51 Barwell Bussiness Park, Leatherhead Road, Chessington, Surrey, KT9 2NY, UK.

FIGURE CAPTIONS

Figure 1

HiBi fibre cross-sectional geometry: (a) Panda and TruePhase fibres, (b) bow tie fibre, (c) D cladding and elliptical core fibre, (d) elliptical core fibre, (e) elliptical cladding, and (f) polarisation axes configuration. The approximate dimensions of the fibres, in μm, are also provided in the figures and all fibres have an outer cladding diameter of 125 μm with the exception of (e) that has a diameter of 80 μm. SAP: stress applying parts. All the dimensions, with the exception of the core diameters (provided by the manufacturers), were measured using an optical microscope that had an image shearing facility.

Figure 2

Loading fixture used to apply uniform transverse strain to HiBi FBG sensors.

Figure 3

Schematic of the interrogation system. SLD: super luminescent diode; FFP-TF: scanning HiBi fibre coupled Fabry-Perot tunable filter; PS: fibre polarisation splitter; DAQ: data acquisition.

Figure 4

Comparison of the maximum and minimum sensitivities to transverse strain for FBGs in the elliptical core and clad fibre. ♦: Elliptical clad slow axis; ■: elliptical clad fast axis; ▲: elliptical core slow axis;×: elliptical core fast axis.

Figure 5

Comparison of the maximum and minimum sensitivities to transverse strain for FBGs in the stress rod induced HiBi fibres i.e. Panda and TruePhase fibres. ♦: Panda slow axis; ■: Panda fast axis; ▲: TruePhase slow axis;×: TruePhase fast axis.

Figure 6

Comparison of the maximum and minimum sensitivities to transverse strain for FBGs in Bow tie (stress induced) and D-clad (geometric induced) HiBi fibres. ♦: Bow tie slow axis; ■: Bow tie fast axis; ▲: D-clad slow axis;×: D-clad fast axis.

Figure 7

Transverse strain sensitivity plotted against angle of rotation for FBG sensors in bow tie fibre.

Figure 8

Transverse strain sensitivity plotted against angle of rotation for FBG sensors in elliptical clad fibre.

Figure 9

Transverse strain sensitivity plotted against angle of rotation for FBG sensors in Panda fibre.

Figure 10

Temperature response of the D - clad fibre. ■: Fast axis; ▲: slow axis.

Figure 11

Temperature response of the elliptical core fibre. ■: Fast axis; ▲: slow axis.

Figure 12

Temperature response of the TruePhase fibre. ■: Fast axis; ▲: slow axis.

Figure 13

Temperature response of the Panda fibre. ■: Fast axis; ▲: slow axis.

Figure 14

Temperature response of the Bow tie fibre. ■: Fast axis; ▲: slow axis.

Figure 15

Temperature response of the elliptical clad fibre. ■: Fast axis; ▲: slow axis.

TABLE CAPTIONS

Table 1

HiBi fibres investigated.

Table 2

Parameters of the HiBi fibres investigated.

Table 3

Slow and fast axis wavelength separation of FBGs fabricated in different types of HiBi fibre.

Table 4

Maximum and minimum transverse load sensitivities of different HiBi FBG sensors for (a) slow and (b) fast axis.

Table 5

The sensitivities of different HiBi FBG sensors to temperature in the slow and fast axes of the fibre.

FIGURE 1

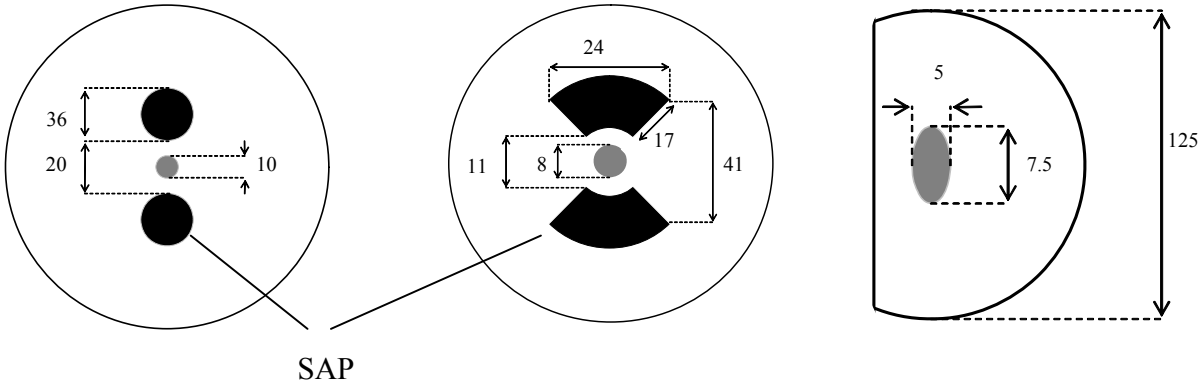

(a) (b) (c)

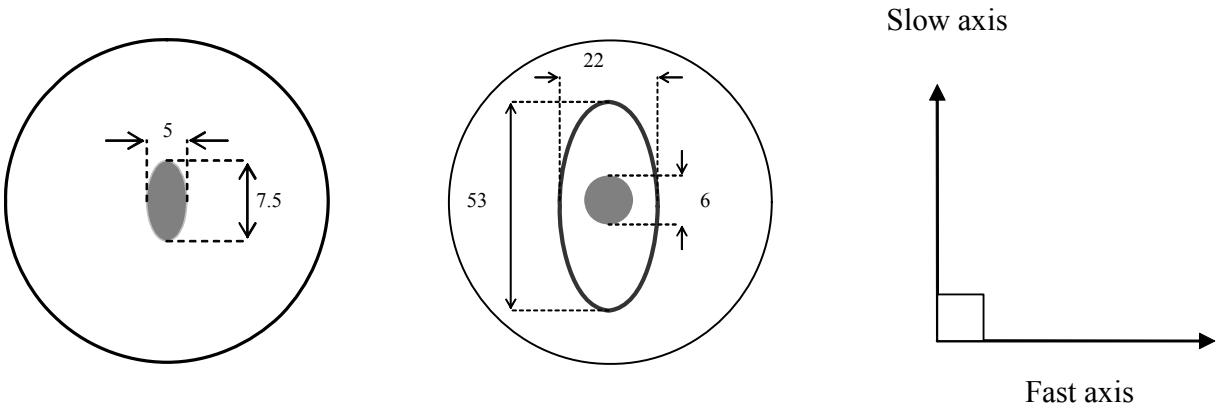

(d) (e) (f)

FIGURE 2

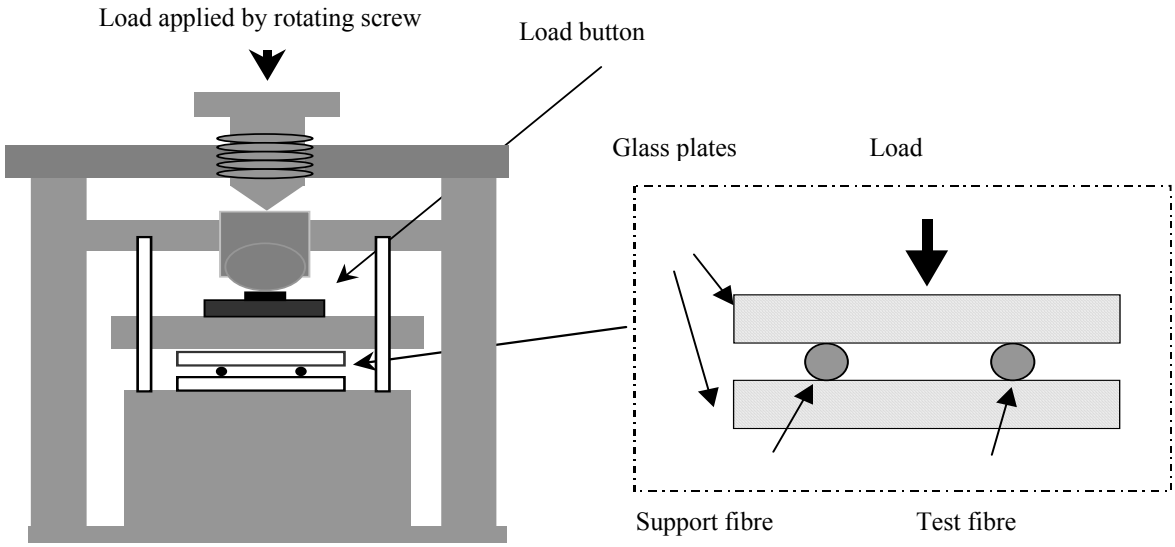
Load applied by rotating screw
Load button
Glass plates
Load
Support fibre
Test fibre

FIGURE 3

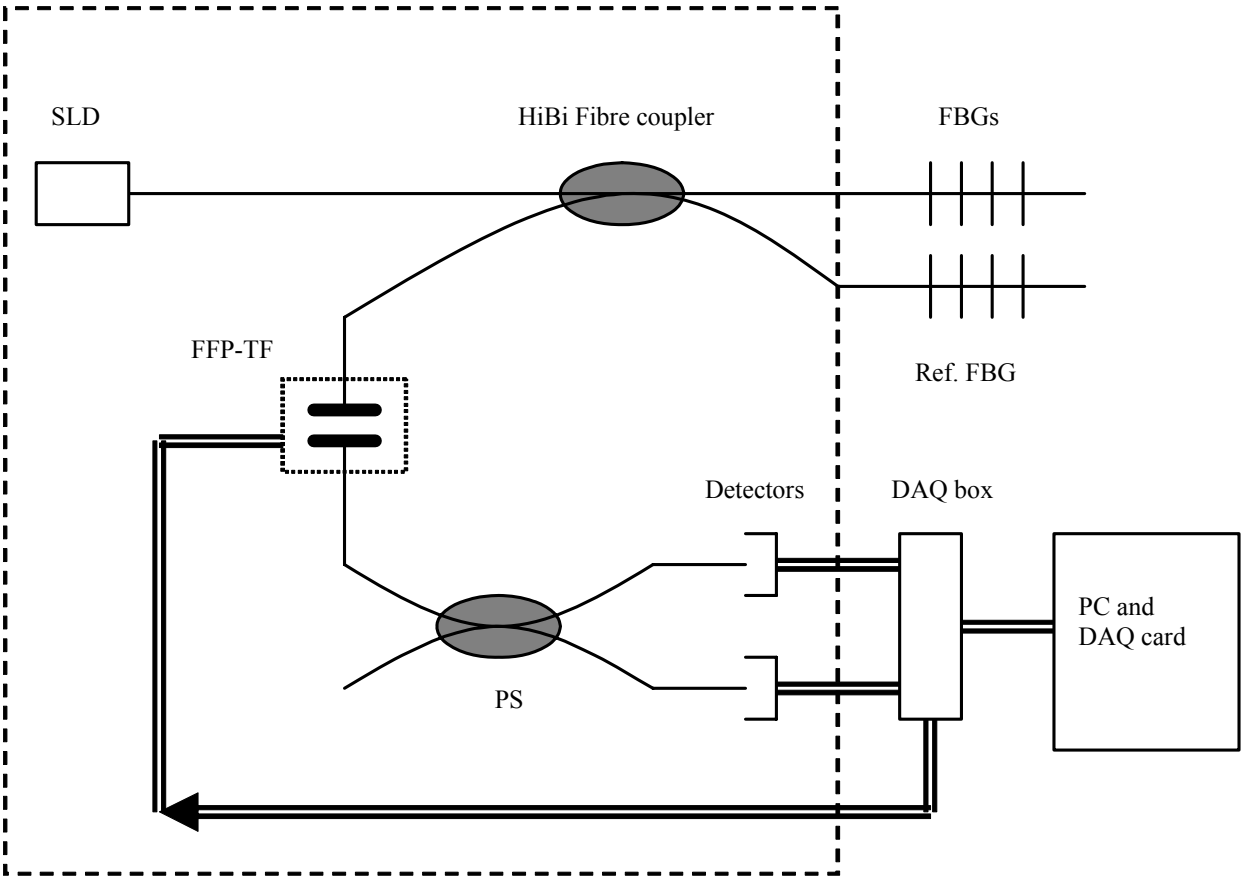
SLD
HiBi Fibre coupler
FBGs
FFP-TF
Ref. FBG
Detectors
DAQ box
PC and
DAQ card
PS

FIGURE 4

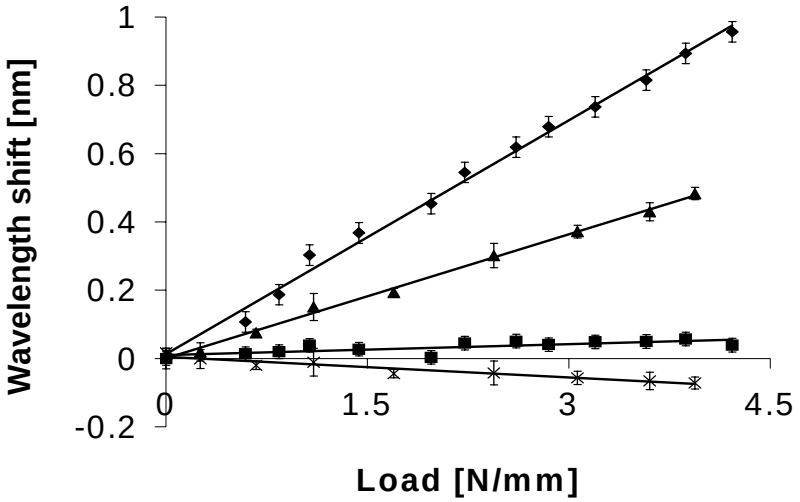

FIGURE 5

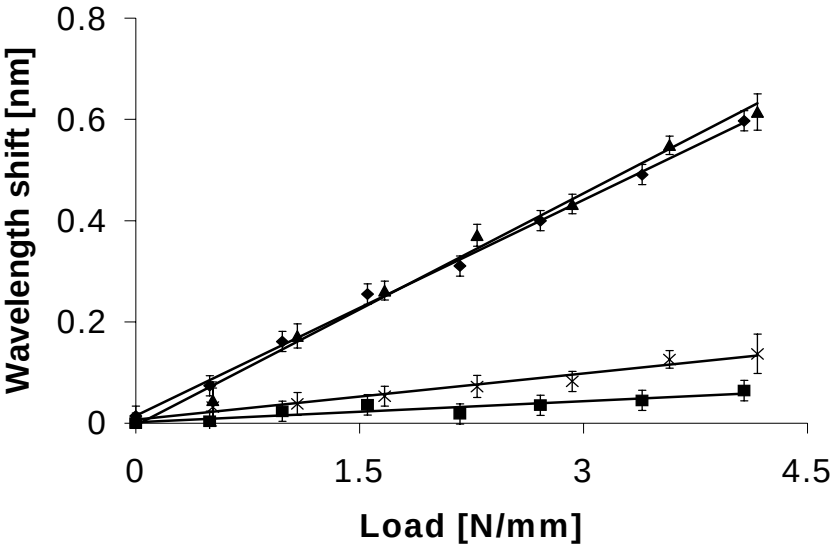

FIGURE 6

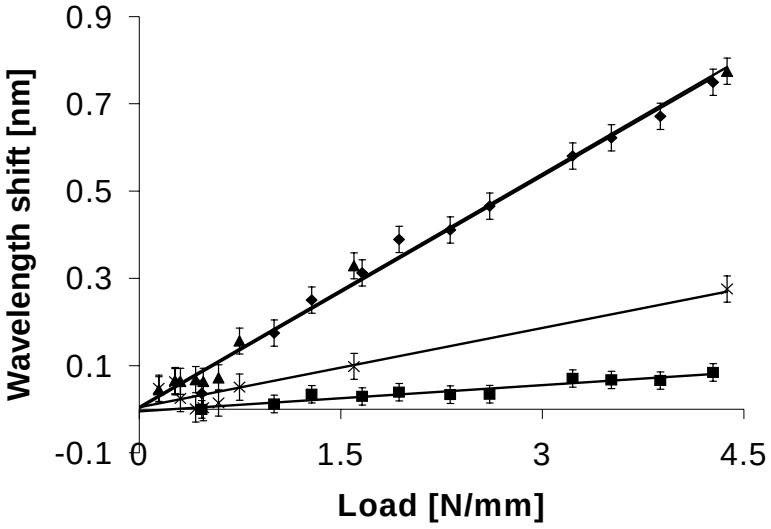

FIGURE 7

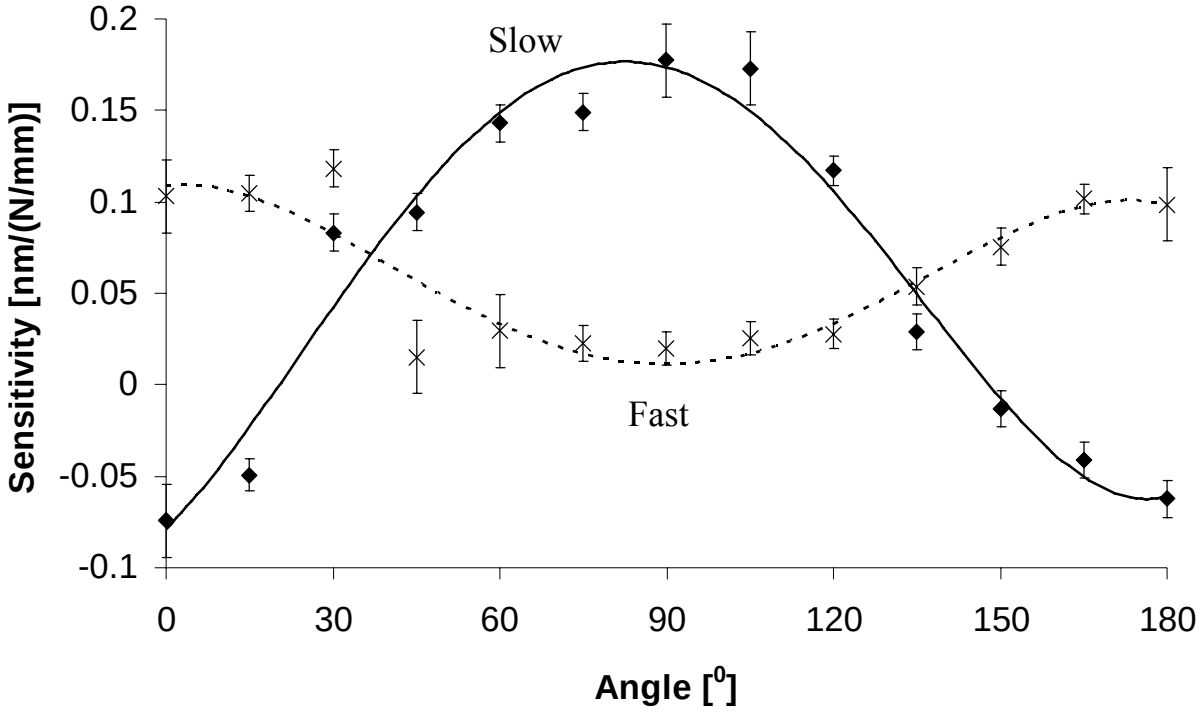
Slow
Fast
Sensitivity [nm/(N/mm)]
Angle [0]
0.2
0.15
0.1
0.05
0
-0.05
-0.1
0
30
60
90
120
150
180

FIGURE 8

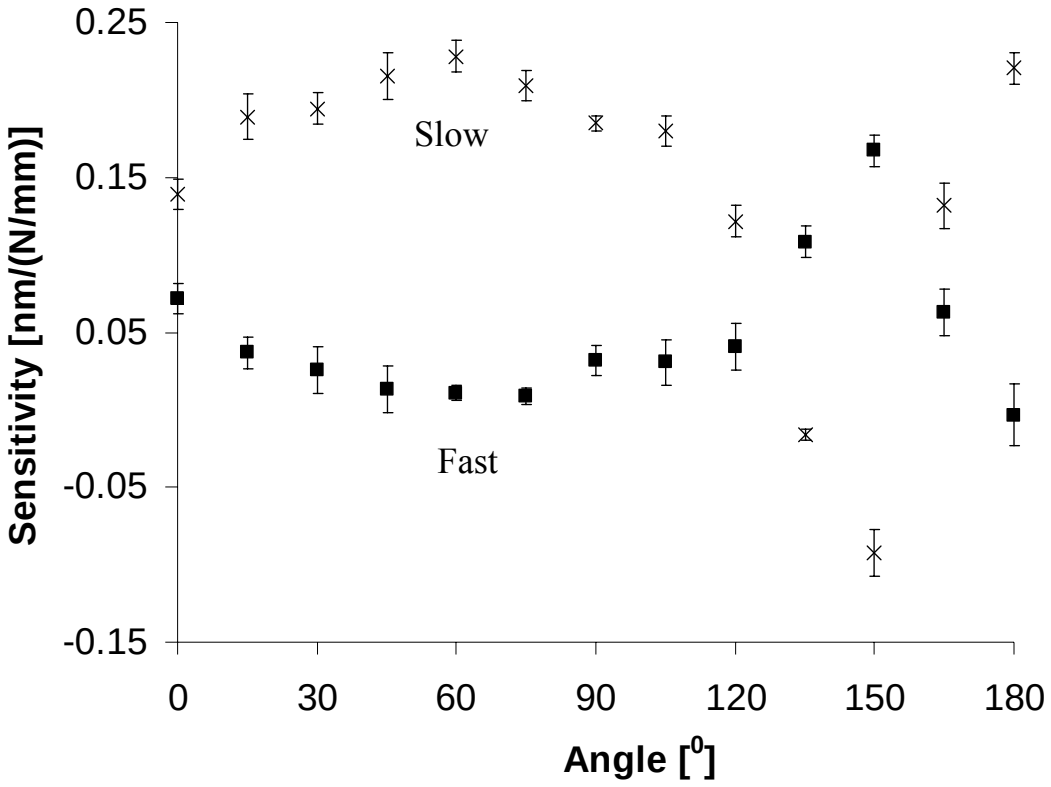
0.25
0.15
0.05
-0.05
-0.15
Sensitivity [nm/(N/mm)]
Slow
Fast
0
30
60
90
120
150
180
Angle [0]

FIGURE 9

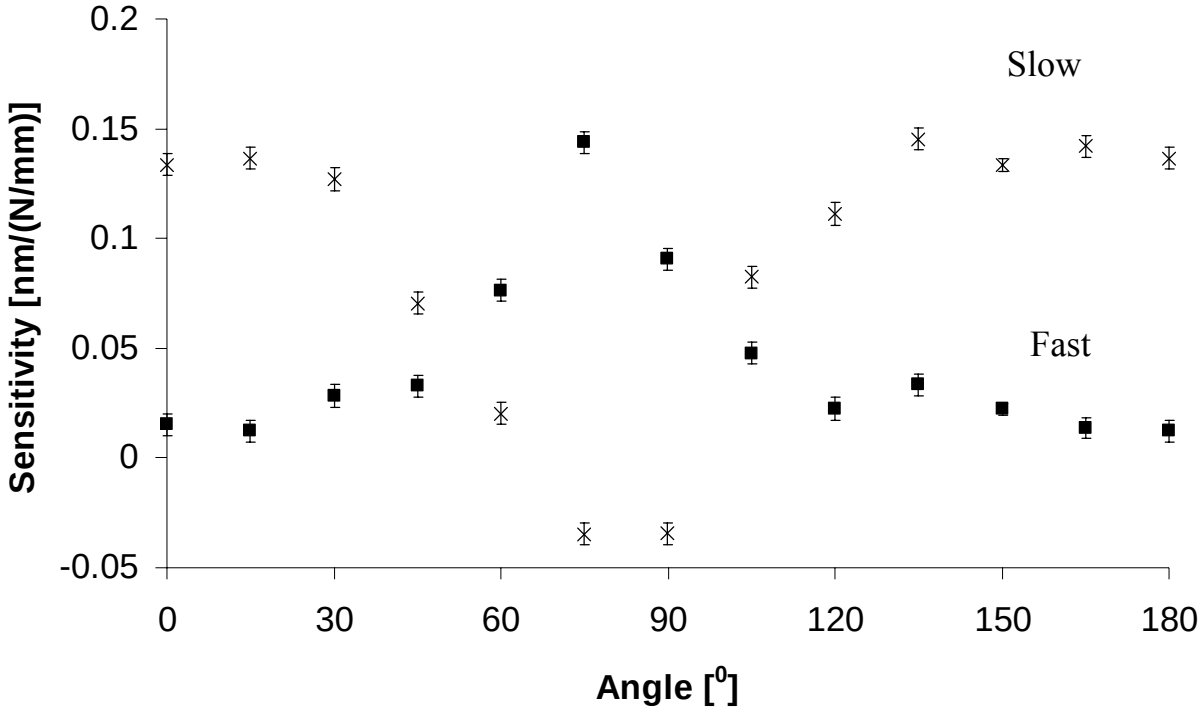
0.2
0.15
0.1
0.05
0
-0.05
Sensitivity [nm/(N/mm)]
Slow
Fast
0
30
60
90
120
150
180
Angle [0]

FIGURE 10

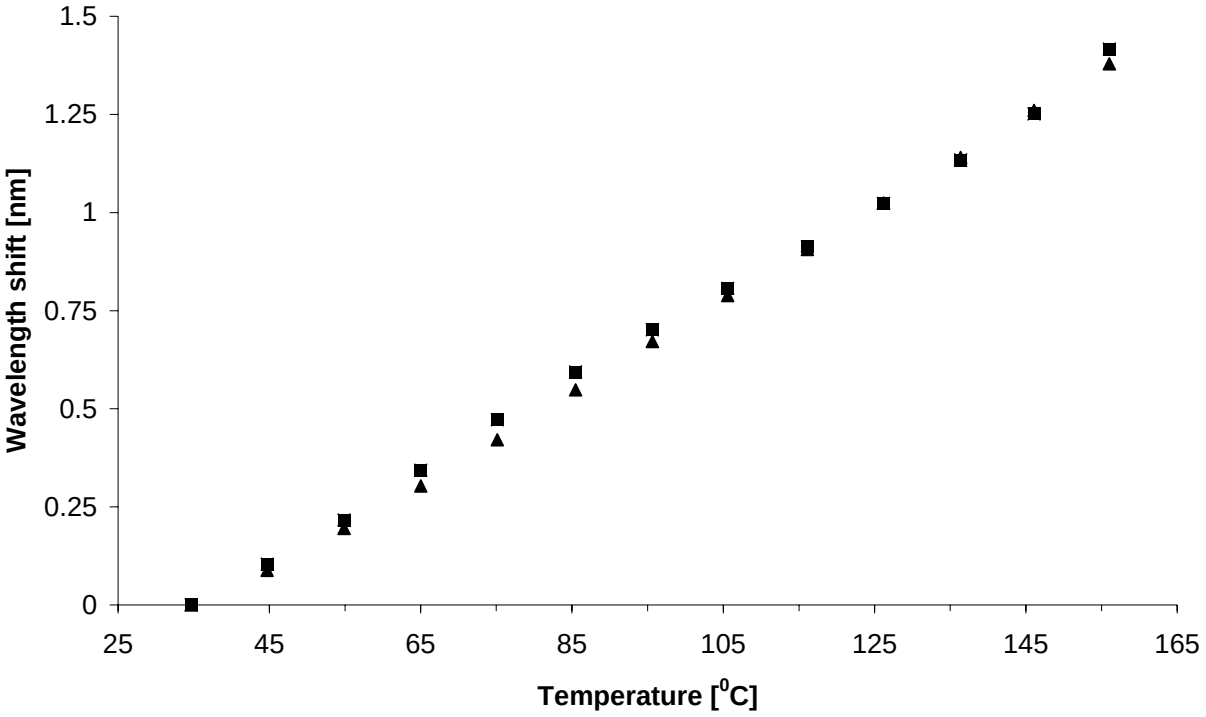
1.5
1.25
1
0.75
0.5
0.25
0
Wavelength shift [nm]
25
45
65
85
105
125
145
165
Temperature [^{0}C]

FIGURE 11

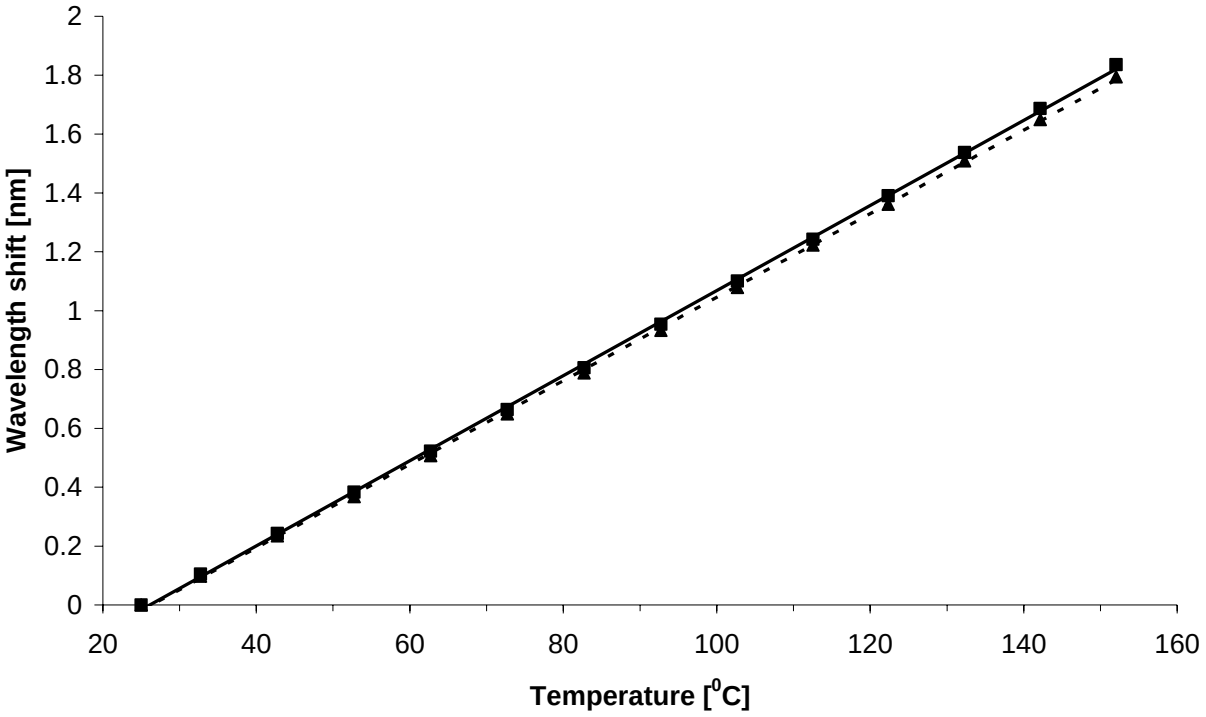
Wavelength shift [nm]
2
1.8
1.6
1.4
1.2
1
0.8
0.6
0.4
0.2
0
20
40
60
80
100
120
140
160
Temperature [^{0}C]

FIGURE 12

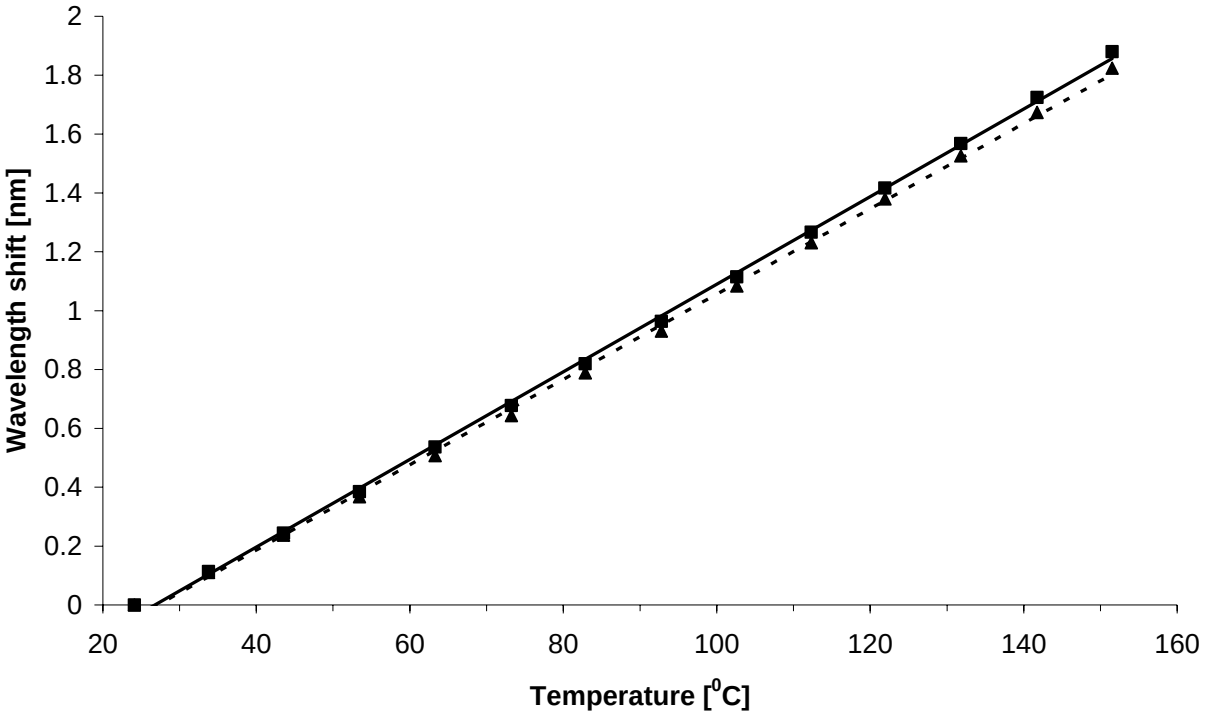
Wavelength shift [nm]
2
1.8
1.6
1.4
1.2
1
0.8
0.6
0.4
0.2
0
20
40
60
80
100
120
140
160
Temperature [^{0}C]

FIGURE 13

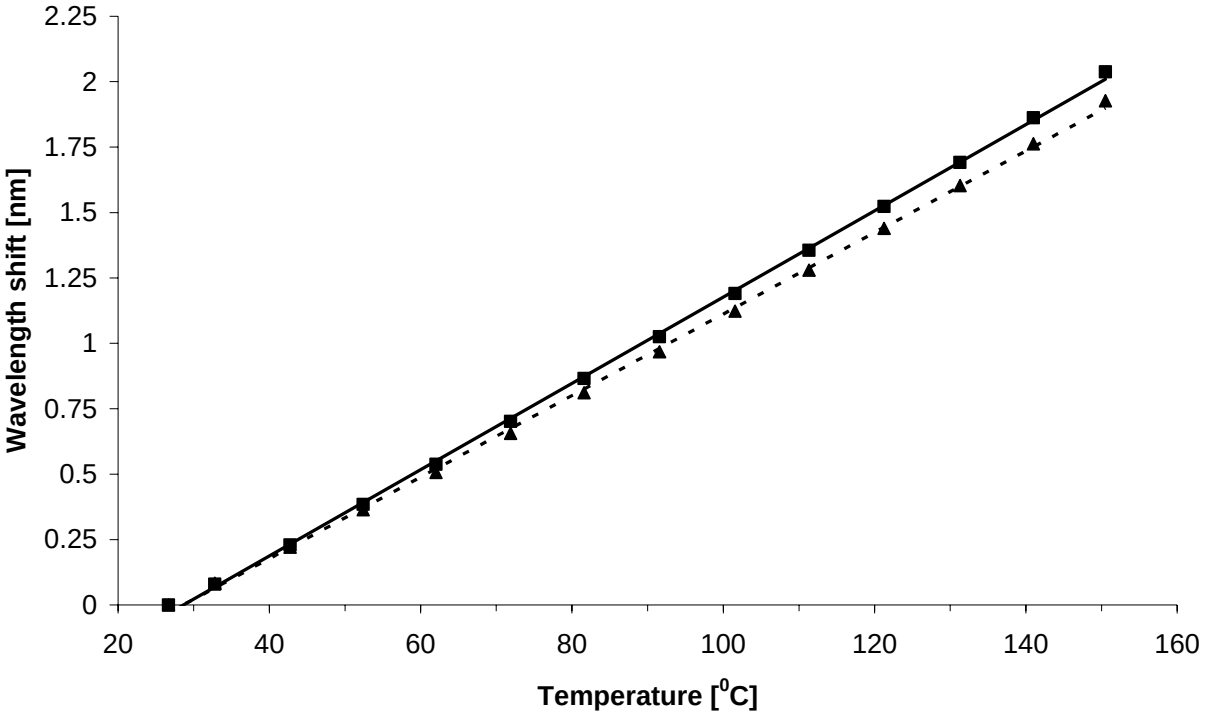
2.25
2
1.75
1.5
1.25
1
0.75
0.5
0.25
0
Wavelength shift [nm]
20
40
60
80
100
120
140
160
Temperature [^{0}C]

FIGURE 14

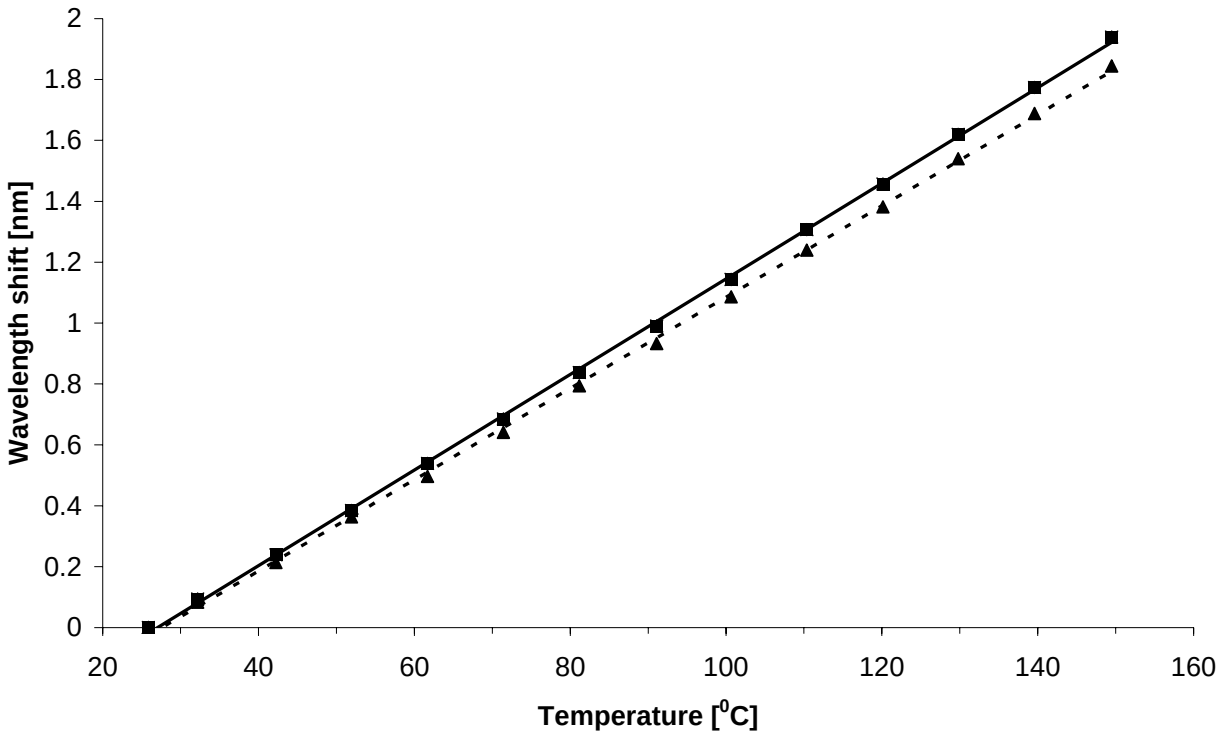
Wavelength shift [nm]
0
0.2
0.4
0.6
0.8
1
1.2
1.4
1.6
1.8
2
20
40
60
80
100
120
140
160
Temperature [^{0}C]

FIGURE 15

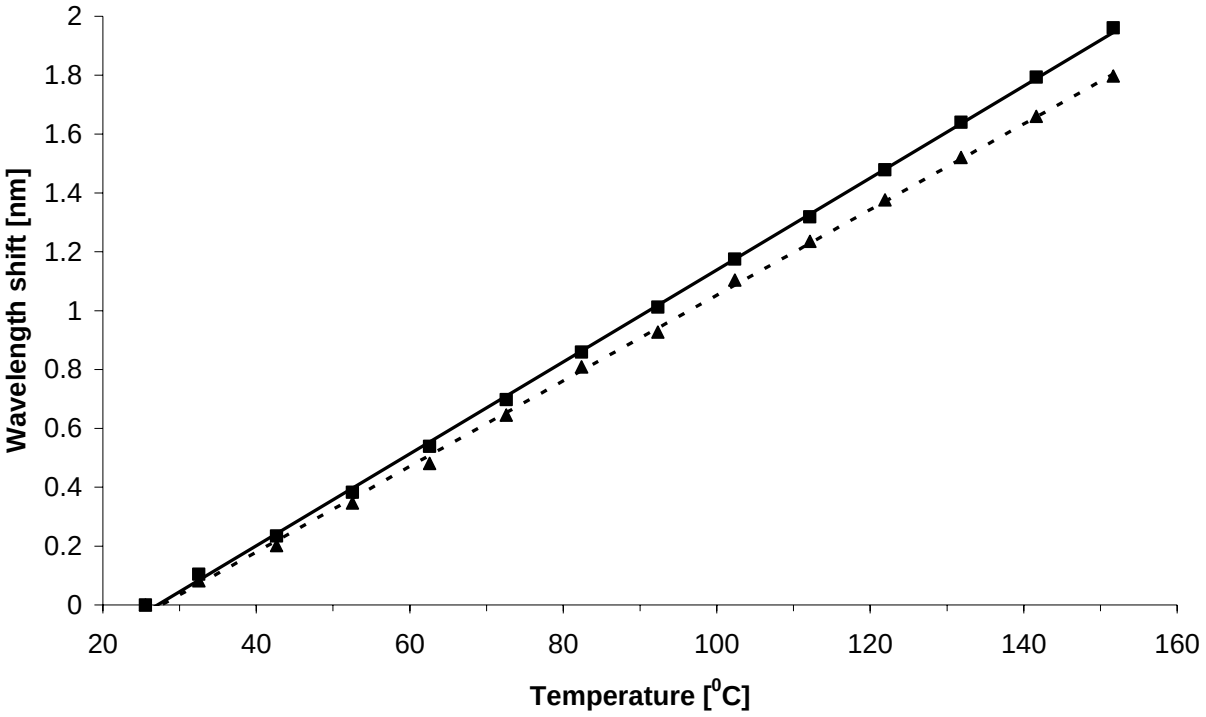
Wavelength shift [nm]
2
1.8
1.6
1.4
1.2
1
0.8
0.6
0.4
0.2
0
20
40
60
80
100
120
140
160
Temperature [^{0}C]

TABLE 1

Fibre Type	Type No.	Manufacturer
D - clad	205170-1550D-5	KVH [30]
Elliptical core	205170-1060S	KVH
TruePhase	BF 06734-01	OFS Fitel [31]
Panda	SM.15-P	Fujikura [32]
Bow tie	HB1500	Fibercore [21]
Elliptical clad	Fs.pm.7811	3M [20]

TABLE 2

Fibre Type	**Cut-off wavelength/nm**	**Cladding diameter/μm**
D - clad	1320	125
Elliptical core	1320	125
TruePhase	1470	125
Panda	1330	125
Bow tie	1275	125
Elliptical clad	1520	80

TABLE 3

Fibre Type	**Nominal Bragg Wavelength/nm**	**Measured peak separation/nm**
D - clad	1556	0.60 ± 0.01
Elliptical core	1550	0.51 ± 0.01
TruePhase	1551	0.56 ± 0.01
Panda	1547	0.34 ± 0.01
Bow tie	1549	0.35 ± 0.01
Elliptical clad	1551	0.54 ± 0.01

TABLE 4

Fibre Type	Slow Axis Sensitivity [nm/(N/mm)] Minimum	Maximum
D - clad	-0.030 ± 0.008	0.18 ± 0.02
Elliptical core	-0.011 ± 0.008	0.12 ± 0.01
TruePhase	-0.038 ± 0.009	0.15 ± 0.02
Panda	-0.035 ± 0.008	0.14 ± 0.01
Bow tie	-0.063 ± 0.008	0.18 ± 0.02
Elliptical clad	-0.092 ± 0.008	0.23 ± 0.02

(a)

Fibre Type	Fast Axis Sensitivity [nm/(N/mm)] Minimum	Maximum
D - clad	0.061 ± 0.009	0.12 ± 0.03
Elliptical core	-0.020 ± 0.008	0.12 ± 0.01
TruePhase	0.030 ± 0.009	0.082 ± 0.009
Panda	0.014 ± 0.007	0.14 ± 0.01
Bow tie	0.020 ± 0.008	0.098 ± 0.008
Elliptical clad	0.011 ± 0.008	0.17 ± 0.01

(b)

TABLE 5

Fibre type	**Slow Axis sensitivity [pm/^{0}C]**	**Fast Axis sensitivity [pm/^{0}C]**
D - clad	11.5 ± 0.1	11.4 ± 0.1
Elliptical core	14.2 ± 0.1	14.5 ± 0.1
TruePhase	14.5 ± 0.1	14.9 ± 0.1
Panda	15.6 ± 0.1	16.5 ± 0.1
Bow tie	15.0 ± 0.1	15.7 ± 0.1
Elliptical clad	14.5 ± 0.1	15.6 ± 0.1